Effects of relativity and configuration interaction on L-shell Auger and radiative decays of the doubly excited $3l3l'$ states of sodiumlike ions

Mau Hsiung Chen
High Temperature Physics Division, Lawrence Livermore National Laboratory, Livermore, California 94550
(Received 24 March 1989)

Auger and radiative transition energies and rates for the states from the $2p^5 3l3l'$ and $2s2p^6 3l3l'$ configurations of the Na-like ions have been calculated for 18 ions with atomic number $18 \le Z \le 92$ using the multiconfiguration Dirac-Fock method. The Z dependence of the transition rates for a few selected states has been analyzed. Numerous irregularities are present in many transitions due to the level-crossing interaction. The effects of relativity and configuration interaction are simultaneously important for medium and heavy ions. These effects can sometimes change the rates for weak transitions by orders of magnitude. Strong configuration interaction between states from the $2p^5 3p^2$ and $2p^5 3s3d$ configurations has been found. Inclusion of the Breit interaction in calculations of the Auger matrix elements can change the Auger rates by as much as a factor of 2. The spin-orbit mixing and Breit interaction are responsible for the decay of most of the quartet states. In particular, the $2p^5 3s3p\ ^4D_{7/2}$ metastable state of low-Z ions decays predominantly by Auger-electron emission via the magnetic interaction.

I. INTRODUCTION

Energy levels and transition rates of multiply ionized atoms are important atomic parameters in the studies of atomic collisions and in the modeling of astrophysical and laboratory-produced plasmas. Auger and x-ray spectra of a few electron ions have previously been investigated.[1-7] The effect of relativity has been found to alter significantly the transition rates of some of the autoionizing states.[6,7]

Auger and radiative transition rates for the $2p^5 3l3l'$ and $2s2p^6 3l3l'$ states of the Na-like phosphorus and krypton have been studied theoretically.[8,9] Recently, Auger spectra from Na-like Ar^{7+} and Fe^{15+} ions have been observed in ion-atom collision experiments.[10,11] Some of the Auger lines have been identified. Although the Auger and radiative transition rates for these doubly excited states have been included in calculations of the dielectronic recombination rate coefficients,[12-14] detailed analysis of the characteristics of the transition rates has never been carried out except for the Kr^{25+} ion.[9]

In this paper we report on the systematic relativistic calculations of Auger and x-ray energies and transition rates for the $2p^5 3l3l'$ and $2s2p^6 3l3l'$ states of the Na-like ions. The calculations were carried out in the intermediate coupling with configuration interaction within the same complex using the multiconfiguration Dirac-Fock method (MCDF).[7,15] The theoretical study covers ions in the range $18 \le Z \le 92$. We pay special attention to the effects of relativity and Breit interaction on the Auger transition rates. The effect of level-crossing interaction on the systematic trends of the transition rates is also investigated.

II. THEORETICAL METHOD

Calculations of Auger and radiative transition rates based on the MCDF method have previously been presented in Ref. 7. Here, we only outline the essential features.

The Auger transition rate is given in perturbation theory by

$$T = \frac{2\pi}{\hbar} \left| \left\langle \Psi_f \left| \sum_{\substack{\alpha,\beta \\ \alpha<\beta}} V_{\alpha\beta} \right| \Psi_i \right\rangle \right|^2 \rho(\varepsilon) \ . \tag{1}$$

Here, Ψ_i and Ψ_f are the antisymmetrized many-electron wave functions of the initial and final states of the ion, respectively; $\rho(\varepsilon)$ is the energy density of final states; and $V_{\alpha\beta}$ is the two-electron interaction operator.

In this work, the two-electron operator $V_{\alpha\beta}$ is taken to be the sum of Coulomb and generalized Breit operator:[16,17]

$$V_{12} = \frac{1}{r_{12}} - \boldsymbol{\alpha}_1 \cdot \boldsymbol{\alpha}_2 \frac{\cos(\omega r_{12})}{r_{12}} + (\boldsymbol{\alpha}_1 \cdot \boldsymbol{\nabla}_1)(\boldsymbol{\alpha}_2 \cdot \boldsymbol{\nabla}_2) \frac{\cos(\omega r_{12}) - 1}{\omega^2 r_{12}} \ , \tag{2}$$

where $\mathbf{r}_1$ and $\mathbf{r}_2$ are position vectors, $r_{12} = |\mathbf{r}_1 - \mathbf{r}_2|$ and $\boldsymbol{\nabla}_1$ and $\boldsymbol{\nabla}_2$ are gradient operators corresponding to $\mathbf{r}_1$ and $\mathbf{r}_2$ respectively. The $\boldsymbol{\alpha}_i$ are Dirac matrices and ω is the wave number of the exchanged virtual photon. In Eq. (2) and hereafter, atomic units are used unless specified otherwise.

In the MCDF method,[15] an atomic-state function can be expanded in terms of configuration-state functions (CSF's). The Auger matrix element can then be written as a sum of matrix elements between two CSF's.[7] The CSF matrix elements can be separated into angular parts and radial integrals using tensor algebra.[18]

The relativistic radiative transition probability is calculated from perturbation theory. The probability for a discrete transition $i \to f$ in multipole expansion is given by[7,19]

TABLE I. Calculated L-shell Auger energies (in eV) and rates (in sec^{-1}) for states from the $2p^5 3s^2$ and $2p^5 3s 3p$ configurations of Ar^{7+}, Ti^{11+}, and Fe^{15+} ions. (Numbers in brackets are powers of 10.)

Initial state	Ar^{7+} Energy	Ar^{7+} Rate	Ti^{11+} Energy	Ti^{11+} Rate	Fe^{15+} Energy	Fe^{15+} Rate
			$2p^5 3s^2$			
$^2P_{3/2}$	100.58	1.02[12]	157.48	2.08[12]	224.10	2.74[12]
$^2P_{1/2}$	102.78	1.02[12]	163.24	2.00[12]	236.63	2.54[12]
			$2p^5 3s 3p$			
$(^3P)^4S_{3/2}$	112.23	1.11[7]	175.28	4.54[7]	248.49	2.90[7]
$(^3P)^4D_{7/2}$	114.09	3.08[5]	178.02	1.69[6]	252.53	5.44[6]
$(^3P)^4D_{5/2}$	114.28	3.32[7]	178.02	8.67[9]	251.74	2.97[10]
$(^3P)^4D_{3/2}$	114.66	4.93[8]	178.67	2.93[10]	252.59	1.24[11]
$(^3P)^4D_{1/2}$	115.17	9.64[9]	179.72	1.30[9]	254.15	2.85[10]
$(^3P)^4P_{5/2}$	115.59	9.21[8]	180.30	3.10[10]	255.59	1.01[11]
$(^3P)^4P_{3/2}$	115.91	2.55[9]	180.63	5.39[10]	255.73	1.23[11]
$(^3P)^4P_{1/2}$	116.36	1.90[11]	181.90	1.47[9]	257.87	9.85[10]
$(^1P)^2D_{3/2}$	117.10	4.15[9]	184.48	4.49[10]	266.65	1.24[10]
$(^1P)^2P_{1/2}$	117.30	1.83[10]	183.96	4.07[10]	263.76	9.87[10]
$(^1P)^2D_{5/2}$	117.76	4.30[9]	185.75	6.95[10]	266.65	2.78[11]
$(^1P)^2P_{3/2}$	117.92	1.74[8]	185.52	1.64[8]	265.05	8.79[10]
$(^1P)^2S_{1/2}$	118.51	9.53[11]	185.43	6.88[12]	264.65	2.15[13]
$(^3P)^2D_{5/2}$	122.51	4.99[11]	189.50	5.28[11]	267.68	5.57[11]
$(^3P)^2D_{3/2}$	123.38	2.12[11]	190.93	1.37[11]	268.90	1.14[11]
$(^3P)^2P_{3/2}$	125.04	2.89[11]	195.65	3.65[11]	279.82	4.59[11]
$(^3P)^2P_{1/2}$	125.15	5.58[12]	195.14	1.71[13]	277.71	4.54[13]
$(^3P)^2S_{1/2}$	130.14	3.08[14]	202.43	3.68[14]	286.94	3.78[14]

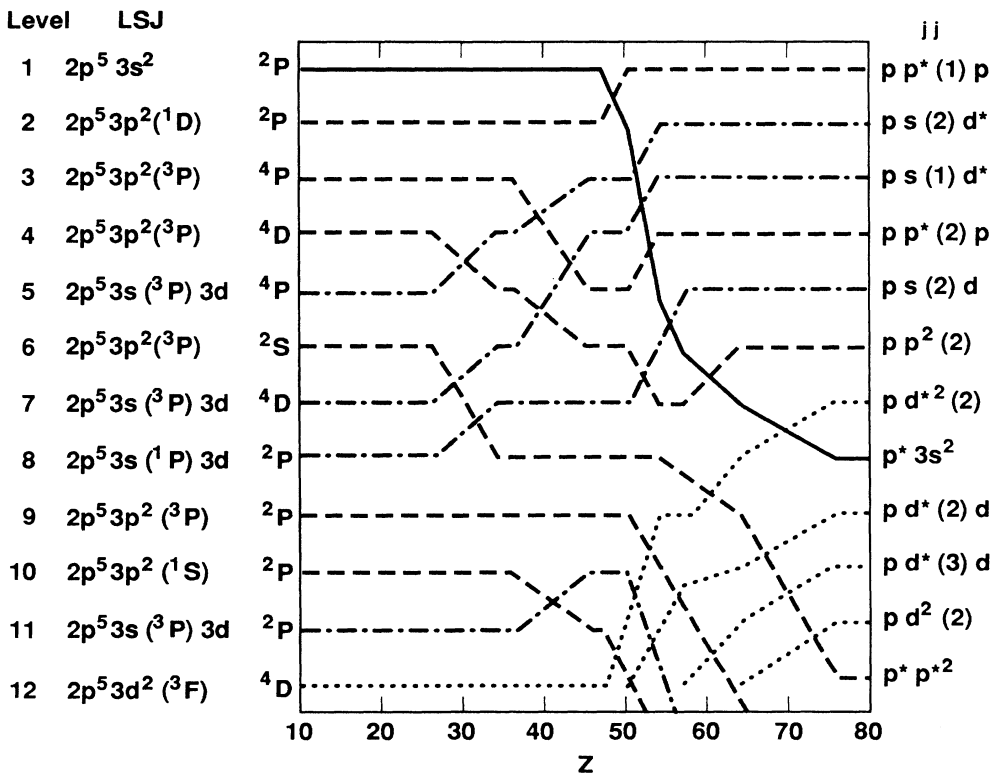

FIG. 1. Lowest odd levels with $J = \frac{1}{2}$ in the complex $2l^{-1}3l'3l''$ of the Na-like ions. The levels are arranged in ascending order of energy.

$$W_{fi}=\frac{1}{2J_i+1}\sum_{M_i,M_f}2\pi\left|\sum_{L,M}\langle f|T_{LM}|i\rangle\right|^2 . \quad (3)$$

In the MCDF model,[7,19] the Lth multipole matrix element $\langle f|T_{LM}|i\rangle$ can be expressed in terms of a CSF basis which can then be written as a sum of products of angular factors and the one-electron matrix elements.[19]

III. NUMERICAL CALCULATIONS

The energies and wave functions for bound states were calculated using the MCDF model with average-level scheme.[15] For the odd-parity states we used 121 CSF's from $2s^22p^53s^2$, $2s^22p^53p^2$, $2s^22p^53s3d$, $2s^22p^53d^2$, $2s2p^63s3p$, and $2s2p^63p3d$ configurations. For the even-parity states, we employed 116 CSF's from $2s^22p^53s3p$, $2s^22p^53p3d$, $2s2p^63s^2$, $2s2p^63s3d$, $2s2p^63p^2$, and $2s2p^63d^2$ configurations. The eigenvectors and energies were obtained by diagonalizing the energy matrix which includes Coulomb interaction, transverse Breit interaction, and the quantum-electrodynamics corrections.[15]

The transition energies were obtained by performing separate MCDF calculations for the initial and final ionic states. The transition rates, however, were calculated using the one-electron wave functions from the initial state to avoid the complication from nonorthogonality of the initial and final orbital wave functions. For highly charged ions, this approximation is expected to yield quite accurate results because of the smallness of the nonorthogonal overlap integrals. The continuum wave functions were generated by solving the Dirac-Fock equations corresponding to the final state without the exchange interaction between bound and continuum electrons. The continuum wave functions were than Schmidt orthogonalized to the initial orbital wave functions.

In order to study the effect of the Breit interaction, the Auger transition rates were calculated according to Eq.

TABLE II. Calculated L-shell x-ray energies (in eV) and rates (in $\sec^{-1}$) for the $2p^53s^2$ and $2p^53s3p$ states of Ar^{7+}, Ti^{11+}, and Fe^{15+} ions. (Numbers in brackets are powers of 10.)

	Ar^{7+}		Ti^{11+}		Fe^{15+}	
Transition	Energy	Rate	Energy	Rate	Energy	Rate
			$2p^53s^2$-$2p^63s$			
$^2P_{3/2}$-$^2S_{1/2}$	243.51	6.94[10]	448.39	2.50[11]	712.79	6.45[11]
$^2P_{1/2}$-$^2S_{1/2}$	245.70	6.99[10]	454.15	2.53[11]	725.31	6.62[11]
			$2p^53s3p$-$2p^63p$			
$(^3P)^4S_{3/2}$-$^2P_{1/2}$	237.78	1.58[8]	440.29	9.75[8]	702.70	2.08[9]
$(^3P)^4D_{3/2}$-$^2P_{1/2}$	240.21	1.54[10]	443.67	1.10[11]	706.79	4.22[11]
$(^3P)^4D_{1/2}$-$^2P_{1/2}$	240.72	1.14[10]	444.73	1.13[11]	708.36	4.58[11]
$(^3P)^4P_{3/2}$-$^2P_{1/2}$	241.46	2.16[10]	445.63	7.59[10]	709.94	1.42[11]
$(^3P)^4P_{1/2}$-$^2P_{1/2}$	241.91	5.77[9]	446.90	1.32[10]	712.08	2.68[10]
$(^1P)^2D_{3/2}$-$^2P_{1/2}$	242.65	4.09[10]	449.49	1.30[11]	719.26	3.40[11]
$(^1P)^2P_{1/2}$-$^2P_{1/2}$	242.85	2.62[10]	448.96	5.87[10]	717.97	1.19[11]
$(^1P)^2P_{3/2}$-$^2P_{1/2}$	243.47	1.90[10]	450.52	3.72[10]	720.86	2.21[9]
$(^1P)^2S_{1/2}$-$^2P_{1/2}$	244.06	5.77[10]	450.43	1.96[11]	718.85	4.17[11]
$(^3P)^2D_{3/2}$-$^2P_{1/2}$	248.93	4.03[10]	455.93	1.26[11]	723.11	3.22[11]
$(^3P)^2P_{3/2}$-$^2P_{1/2}$	250.59	3.58[9]	460.65	2.51[10]	734.03	7.42[10]
$(^3P)^2P_{1/2}$-$^2P_{1/2}$	250.70	2.97[10]	460.15	5.86[10]	731.92	3.42[10]
			$2p^53s3p$-$2p^63p$			
$(^3P)^2S_{1/2}$-$^2P_{1/2}$	255.69	3.37[10]	467.44	1.48[11]	741.14	4.55[11]
$(^3P)^4S_{3/2}$-$^2P_{3/2}$	237.45	6.27[8]	439.22	3.64[9]	700.11	9.57[9]
$(^3P)^4D_{5/2}$-$^2P_{3/2}$	239.50	5.94[9]	441.96	2.84[10]	703.36	7.78[10]
$(^3P)^4D_{3/2}$-$^2P_{3/2}$	239.88	9.90[7]	442.61	4.72[8]	704.21	3.78[8]
$(^3P)^4D_{1/2}$-$^2P_{3/2}$	240.39	2.06[9]	443.66	8.01[9]	705.78	1.19[10]
$(^3P)^4P_{5/2}$-$^2P_{3/2}$	240.81	1.84[10]	444.24	9.44[10]	707.21	2.87[11]
$(^3P)^4P_{3/2}$-$^2P_{3/2}$	241.13	2.94[10]	444.57	1.45[11]	707.36	4.33[11]
$(^3P)^4P_{1/2}$-$^2P_{3/2}$	241.58	9.06[9]	445.84	1.64[11]	709.49	6.06[11]
$(^1P)^2D_{3/2}$-$^2P_{3/2}$	242.32	4.95[9]	448.42	5.23[8]	716.67	9.78[9]
$(^1P)^2P_{1/2}$-$^2P_{3/2}$	242.51	4.38[10]	447.90	8.87[10]	715.38	8.96[10]
$(^1P)^2D_{5/2}$-$^2P_{3/2}$	242.98	7.12[10]	449.69	2.02[11]	718.27	8.00[10]
$(^1P)^2P_{3/2}$-$^2P_{3/2}$	243.14	4.57[10]	449.46	1.31[11]	718.27	1.62[11]
$(^1P)^2S_{1/2}$-$^2P_{3/2}$	243.73	3.80[10]	449.37	4.02[10]	716.27	7.77[9]
$(^3P)^2D_{5/2}$-$^2P_{3/2}$	247.73	4.24[10]	453.44	1.68[11]	719.31	8.27[11]
$(^3P)^2D_{3/2}$-$^2P_{3/2}$	248.60	1.98[10]	454.87	1.12[11]	720.52	4.33[11]
$(^3P)^2P_{3/2}$-$^2P_{3/2}$	250.25	5.16[10]	459.59	1.53[11]	731.44	3.62[11]
$(^3P)^2P_{1/2}$-$^2P_{3/2}$	250.37	4.53[10]	459.08	2.13[11]	729.33	7.05[11]
$(^3P)^2S_{1/2}$-$^2P_{3/2}$	255.35	3.41[10]	466.37	9.42[10]	738.56	1.24[11]

(1) both with and without Breit-interaction terms [second and third terms in Eq. (2)]. The effects of relativistic energies and wave functions on the transition rates were investigated by comparing the MCDF results and the predictions from the nonrelativistic multiconfiguration Hartree-Fock (MCHF) ones. The present MCHF values were obtained by repeating the MCDF calculations with the velocity of light increased by a thousandfold to simulate the nonrelativistic limit.[15]

IV. RESULTS AND DISCUSSION

A systematic calculation of Auger and radiative transition energies and rates for the doubly excited $3l3l'$ states of the Na-like ions has been performed using the MCDF method. The calculated L-shell Auger energies and rates for states from the $2p^5 3s^2$ and $2p^5 3s 3p$ configurations of Ar^{7+}, Ti^{11+}, and Fe^{15+} ions are listed in Table I. The corresponding data for the electric-dipole radiative transitions are listed in Table II. The energy levels for the $3l3l'$ configurations can be identified unambiguously by using LSJ coupling and j-j coupling notations for light and heavy ions, respectively. For medium-Z ions, it is rather difficult to classify the states consistently using the dominant component only because of the complicated level crossings. Instead, we use the energy ordering to assist the classification. Each energy level is identified by the LSJ coupling at low Z, is followed through the isoelectronic sequence by using the energy ordering and nonrelativistic configuration, and then is classified by using j-j coupling at high Z. Under this procedure, states with the same total angular momentum and from the same nonrelativistic configuration will not cross each other. In Fig. 1, the first 12 lowest odd levels with $J=\frac{1}{2}$ in the $2l^{-1}\,3l'3l''$ complex of the Na-like ions are shown. The orbital symbols l and l^* represent levels with $j=l+\frac{1}{2}$ and $j=l-\frac{1}{2}$, respectively. The j-j notation

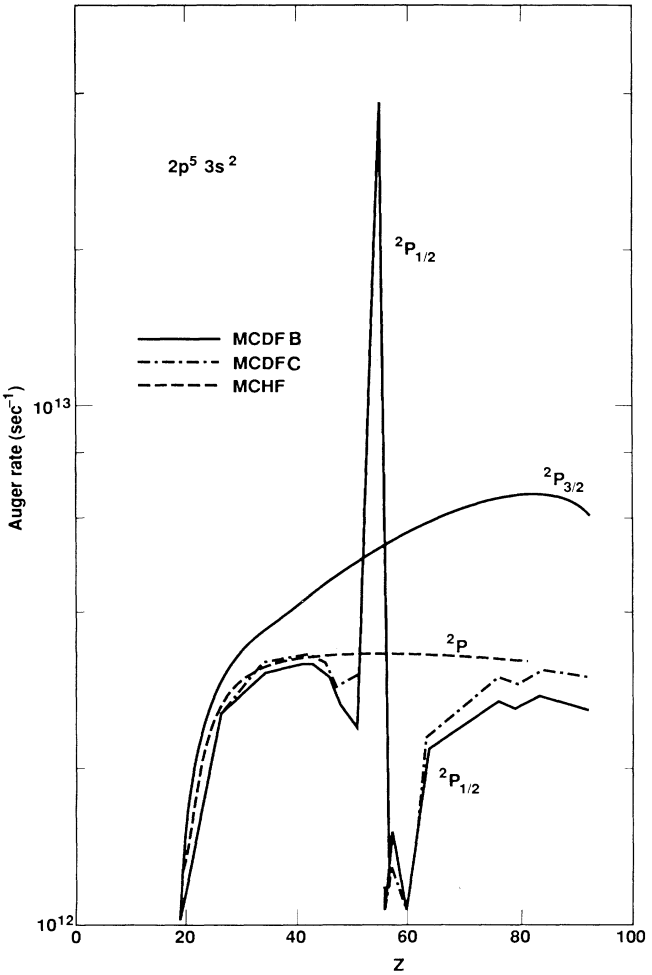

FIG. 2. Calculated Auger rates for the $2p^5 3s^2\,{}^2P$ states as functions of atomic number. The solid curves indicate the results from the MCDF calculations with the Coulomb and Breit interactions for the Auger operator. The dash-dotted curves represent the values from the MCDF calculations with the Coulomb operator only. The dashed curve displays the predictions from the nonrelativistic multiconfiguration Hartree-Fock model. The curves are labeled by the initial states of the transitions. For the $2p_{3/2}$ state, MCDFC coincides with MCDFB.

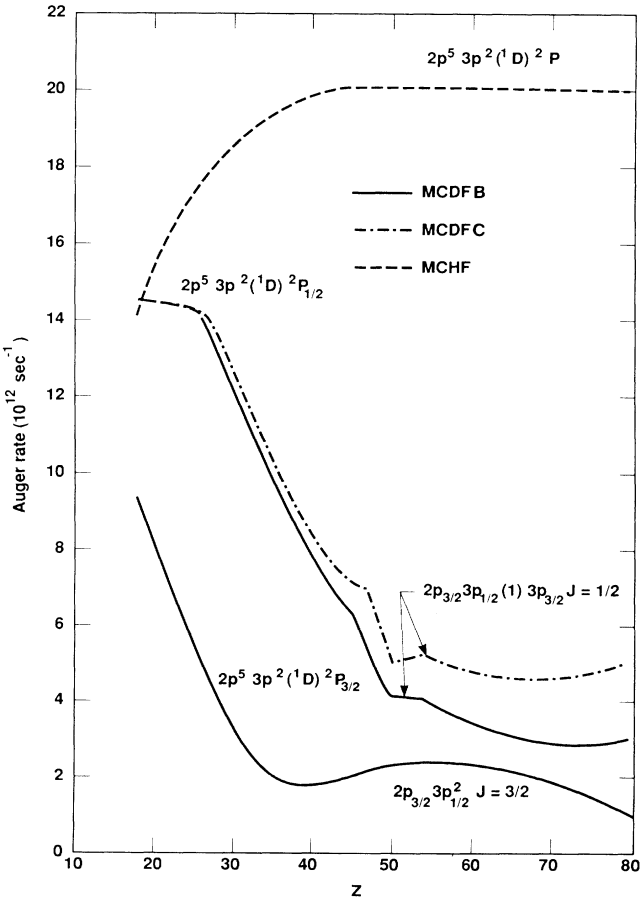

FIG. 3. Calculated Auger rates for the $2p^5 3p^2({}^1D)\,{}^2P$ states. The legend is the same as in Fig. 1. The curves are labeled by the LSJ coupling notations at low Z and by j-j coupling at high Z.

$pp^*(1)p$ means a hole in $2p_{3/2}$ subshell coupled with an electron in the $3p_{1/2}$ state to give an intermediate quantum number 1 and then coupled with another electron in the $3p_{3/2}$ subshell. The levels are arranged in ascending order in energy. For low-Z ions the $2p^5 3s^2\,{}^2P_{1/2}$ state is the lowest level for the $J=\frac{1}{2}$ odd manifold. It comes down to cross seven levels as Z increases from 18 to 79. Similarly, there exist many level crossings for the other $J=\frac{1}{2}$ states. For ions near a certain level crossing, the wave functions of the states involved might become significantly mixed due to the strong configuration interaction. These level-crossing configuration interactions can have very pronounced effects on the systematic trends of the transition rates through the isoelectronic sequence.

Including a local semiclassical exchange interaction[20] in the calculation of the continuum wave function has been found to produce only a few percent change in the Auger transition rate. Hence the neglect of the exchange interaction between bound and continuum electrons is a reasonable approximation in the present work.

The Auger spectra for the Ar^{7+} and Fe^{15+} ions have been observed in the ion-atom collision experiments.[10,11] The theoretical calculated Auger energies have been found to agree quite well with experiments.[10,11] For the Kr^{25+} ion, the Auger rates from the present MCDF method agree satisfactorily with the values obtained using the Stieltjes moment theory[9] for the strong transitions.

The Auger transition rates from the MCDF calculations with Breit interaction (MCDFB) and without Breit interaction (MCDFC) and from the nonrelativistic calculations (MCHF) for a few selected autoionizing states are compared in Figs. 2–5. The radiative transition rates for some states are displayed in Figs. 6 and 7. From these comparisons, we arrive at the following general observations.

(i) Numerous irregularities and sharp discontinuities along the isoelectronic sequence exist in many transitions due to the level-crossing interaction. Sometimes, many irregularities are present in one transition. For example, the Auger transition rate for the $2p^5 3s^2\,{}^2P_{1/2}$ state peaks sharply at $Z=54$ and suffers many irregularities in the range $40<Z<80$ (Fig. 2). The behavior can be traced to the effect of level crossings involving $2p^5 3s^2\,{}^2P_{1/2}$ and the other $2p^5 3p^2$ and $2p^5 3s 3d$ $J=\frac{1}{2}$ states (see Fig. 1). On the other hand, the Auger rate for the $2p^5 3s^2\,{}^2P_{3/2}$ state behaves normally, as expected, since the ${}^2P_{3/2}$ state does not go through any level crossing. Similar behavior is also observed for the radiative transitions of the $2p^5 3s^2\,{}^2P$ states (see Figs. 6 and 7). The Auger transition for the $2p^5 3s({}^1P)3p\,{}^2P_{1/2}$ state is forbidden in LS coupling because it cannot simultaneously satisfy the selection rules for total orbital angular momentum and parity. The Auger rate for this state starts with a small value at low

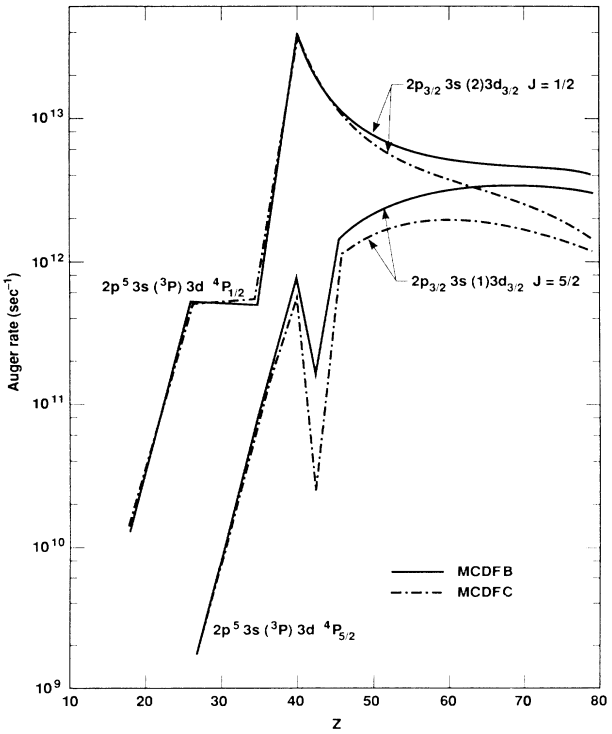

FIG. 4. Calculated Auger rates for the $2p^5 3s({}^3P)3d\,{}^4P$ states. The legend is the same as Fig. 1. The curves are labeled by the LSJ coupling notations at low Z and by j-j coupling at high Z.

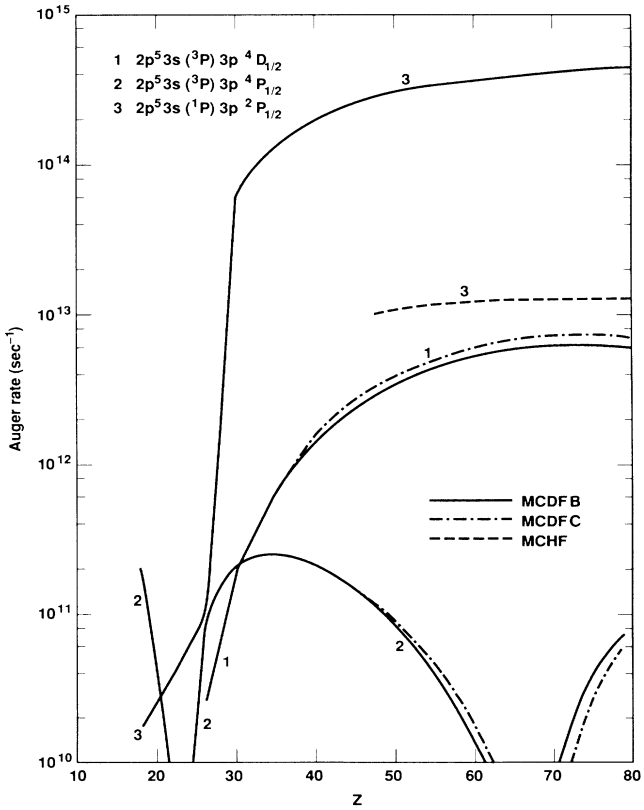

FIG. 5. Calculated Auger rates for the $2p^5 3s({}^3P)3p\,{}^4D_{1/2}$, $2p^5 3s({}^3P)3p\,{}^4P_{1/2}$, and $2p^5 3s({}^1P)3p\,{}^2P_{1/2}$ states as functions of atomic number.

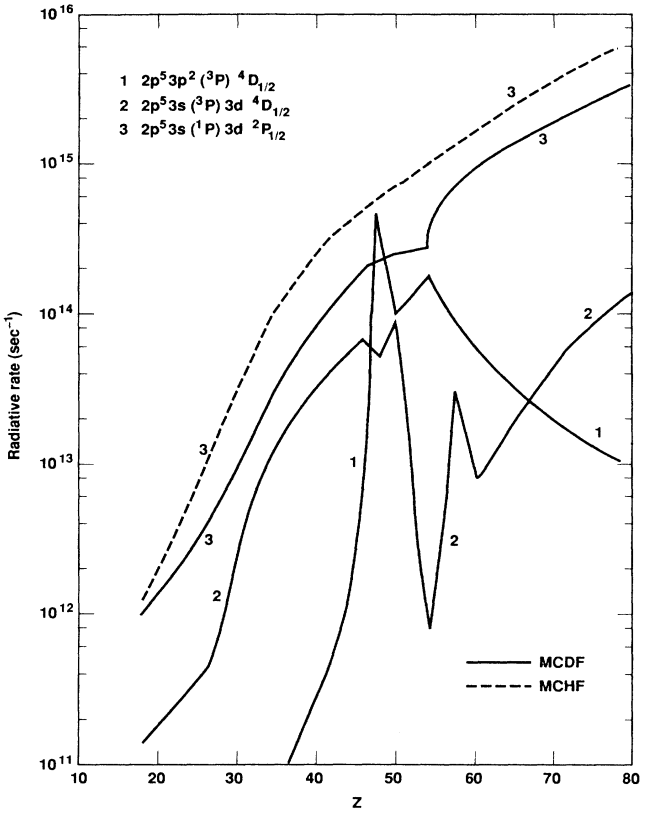

FIG. 6. Radiative transition rates for transitions from the $2p^5 3p^2(^3P)\,^4D_{1/2}$, $2p^5 3s(^3P)3d\,^4D_{1/2}$, and $2p^5 3s(^1P)3d\,^2P_{1/2}$ states to the $2p^6 3s\,^2S_{1/2}$ state as functions of atomic number. The solid curves display the results from the MCDF calculations. The dashed curve represents the values from the nonrelativistic calculations. The curves are labeled by the initial states in the *LSJ* coupling notation.

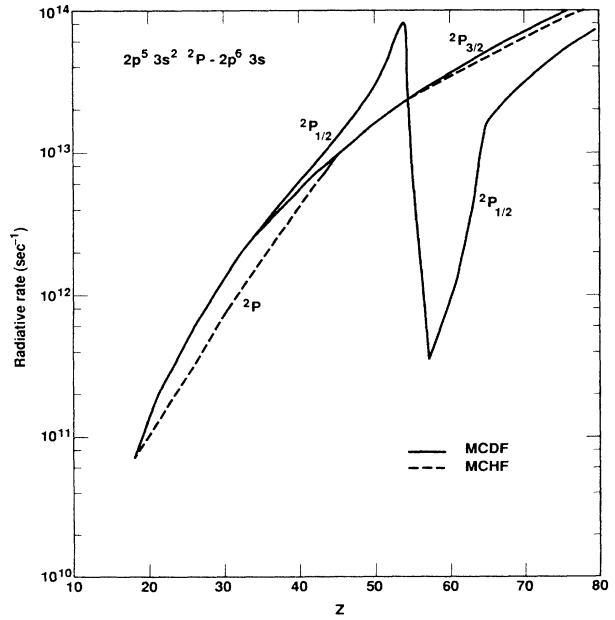

FIG. 7. Radiative rates for the $2p^5 3s^2\,^2P - 2p^6 3s$ transitions. The legend is the same as in Fig. 5.

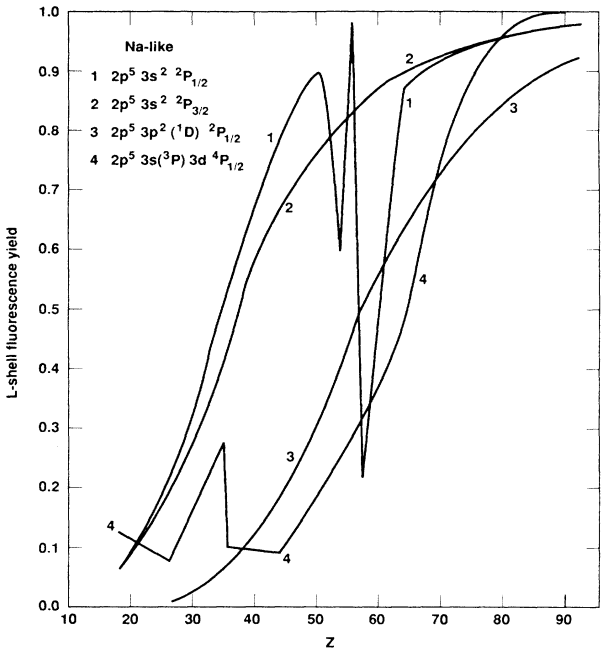

FIG. 8. *L*-shell fluorescence yields for the $2p^5 3s^2\,^2P_{1/2}$, $2p^5 3s^2\,^2P_{3/2}$, $2p^5 3p^2(^1D)\,^2P_{1/2}$, and $2p^5 3s(^3P)3d\,^4P_{1/2}$ states as functions of atomic number.

Z and has a large discontinuity at $Z=30$ due to the level-crossing interaction with the $2p^5 3s(^1P)3p\,^2S_{1/2}$ state (see Fig. 5).

(ii) Strong configuration interaction between states from the $2p^5 3p^2$ and $2p^5 3s 3d$ configurations has been found. The $3 \rightarrow 2$ radiative electric-dipole transition ($E1$)

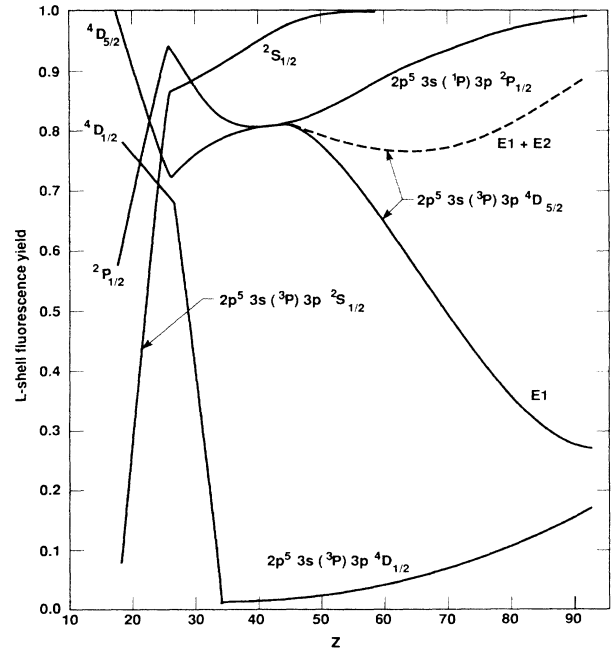

FIG. 9. *L*-shell fluorescence yields for the $2p^5 3s(^1P)3p\,^2P_{1/2}$, $2p^5 3s(^1P)3p\,^2S_{1/2}$, $2p^5 3s(^3P)3p\,^4D_{1/2}$, and $2p^5 3s(^3P)3p\,^4D_{5/2}$ states.

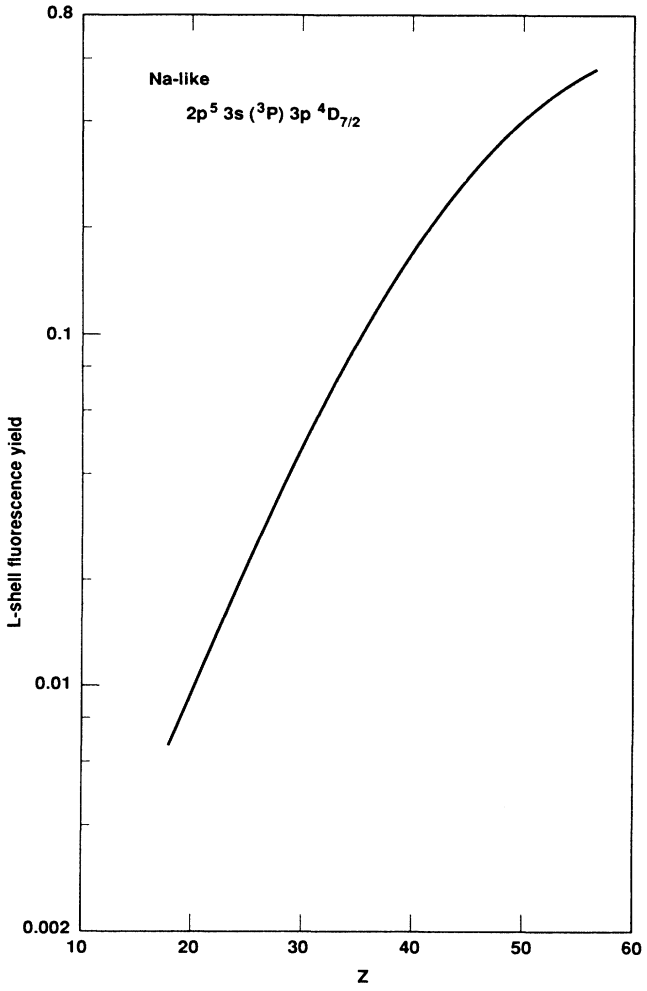

FIG. 10. L-shell fluorescence yields for the $2p^5 3s(^3P)3p\ ^4D_{7/2}$ state.

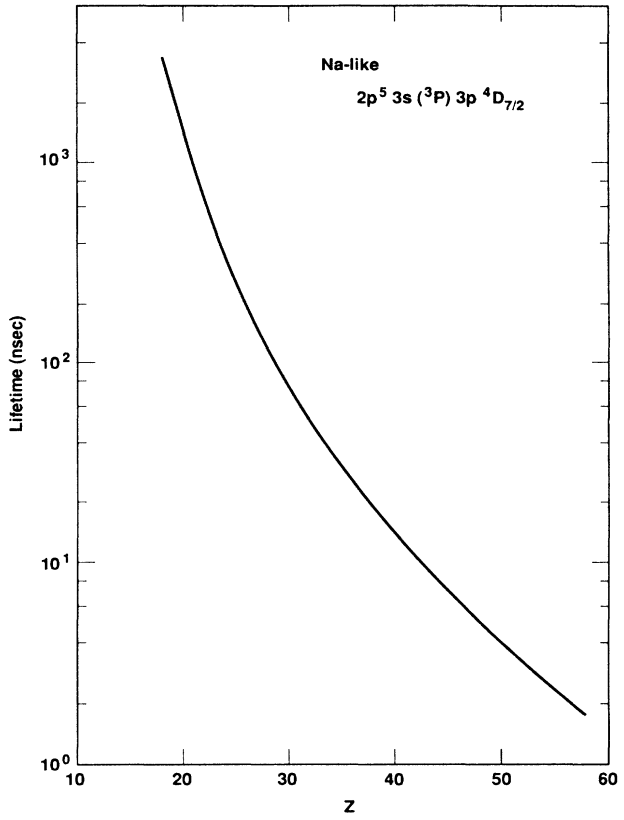

FIG. 11. Lifetime of the $2p^5 3s(^3P)3p\ ^4D_{7/2}$ state.

for the $2p^5 3p^2$ states is forbidden under the single-configuration approximation. However, in the MCDF calculations, the $E1$ transitions for the $2p^5 3p^2$ states become quite prominent for the mid-Z ions because of the strong configuration interaction with the $2p^5 3s 3d$ states (Fig. 6). Furthermore, the irregularities observed in the Z dependence of the transition rates can be explained as due to the effect of level crossings involving states from the $2p^5 3p^2$ and $2p^5 3s 3d$ configurations (see Figs. 1 and 6).

(iii) The effect of relativity changes the level structure and introduces many level crossings, which then lead to irregularities in the Z dependence of the transition rates. The relativistic effect can change the transition rates for the allowed transitions by as much as a factor of 5 (see Figs. 2, 3, 5, and 6).

(iv) Inclusion of the Breit interaction in the calculation of the Auger matrix elements can have quite different effects on various transitions. For some transitions, it can change the Auger rates by as much as a factor of 2. For others, it causes no effect at all. In general, the Breit interaction is more important for the weak transitions than for the strong ones.

(v) The spin-orbit interaction is extremely important. Without it, the $3\rightarrow 2$ $E1$ radiative and Auger transitions for the quartet states are forbidden. Including the spin-orbit mixing, the decay rates for the quartet states can become quite large and the transition rates for the fine-structure states can differ by as much as a factor of 2 for the medium and heavy ions.

In Figs. 8 and 9, the L-shell fluorescence yields for some multiplet states are displayed. As expected, the Z dependence of the fluorescence yields suffers many discontinuities due to the level-crossing interaction. In addition, the electric-quadrupole ($E2$) transition for the $2p^5 3s 3p\ ^4D_{5/2}$ state has been found to increase L-shell fluorescence yield by a factor of 3 at $Z=92$.

The decay characteristics of the $2p^5 3s 3p\ ^4D_{7/2}$ state deserve some special attention. The $2p^5 3s 3p\ ^4D_{7/2}$ state is metastable. It has the largest total angular momentum among states from the $2p^5 3s 3p$ configuration. It is forbidden to decay by $n=3\rightarrow 2$ and $n=3\rightarrow 3$ $E1$ emissions and is also forbidden for Auger transition due to the Coulomb interaction. In addition, it cannot decay by the spin-orbit mixing with the doublet states. However, it can decay via Auger electron emission through the spin-spin, spin-other-orbit, and orbit-orbit interactions which are parts of the Breit interaction and the $n=3\rightarrow 2$ $M2$ radiative transition. The metastability of the $2p^5 3s 3p\ ^4D_{7/2}$ state has been established experimentally for the Ar^{7+} and Fe^{15+} ions.[10,11] The L-shell fluores-

cence yield and the lifetime of the $2p^5 3s 3p\ ^4D_{7/2}$ state are shown in Figs. 10 and 11, respectively. For $Z \leq 30$, the fluorescence yield is less than 0.05. As Z increases to 54, the $M2$ emission becomes as important as the radiationless transition. The lifetimes of the $2p^5 3s 3p\ ^4D_{7/2}$ state for the low- and mid-Z ions are quite long (for example, 180 ns at $Z=26$). Even for ions with Z as high as 54, the lifetime of this metastable state is still 2.3 ns. Measurement of the lifetime for this metastable state is in progress.[21]

ACKNOWLEDGMENTS

This work was performed under the auspices of the U. S. Department of Energy, by the Lawrence Livermore National Laboratory, under Contract No. W-7405-ENG-48.

[1]V. A. Boiko, A. Ya Faenov, and S. A. Pikuz, J. Quant. Spectrosc. Radiat. Transfer **19**, 11 (1978).
[2]C. P. Bhalla, A. H. Gabriel, and L. P. Presnyakov, Mon. Not. R. Astron. Soc. **172**, 359 (1975).
[3]K. T. Cheng, C. P. Lin, and W. R. Johnson, Phys. Lett. **48A**, 437 (1974).
[4]L. A. Vainshtein and U. I. Safronova, At. Data Nucl. Data Tables **21**, 50 (1978).
[5]C. P. Bhalla and T. W. Tunnell, Z. Phys. A **303**, 199 (1981).
[6]M. H. Chen, B. Crasemann, and H. Mark, Phys. Rev. A **24**, 1852 (1981); **27**, 544 (1983); **26**, 1441 (1982).
[7]M. H. Chen, Phys. Rev. A **31**, 1449 (1985).
[8]K. R. Karim, M. H. Chen, and B. Crasemann, Phys. Rev. A **28**, 3355 (1983).
[9]B. Whitten and A. Hazi, Phys. Rev. A **33**, 1039 (1986).
[10]R. Hutton, M. H. Prior, S. Chantrenne, M. H. Chen, and D. Schneider, Phys. Rev. A **39**, 4902 (1989).
[11]D. Schneider, M. H. Prior, R. Hutton, S. Chantrenne, and M. H. Chen (unpublished).
[12]L. J. Roszman, Phys. Rev. A **20**, 673 (1979).
[13]J. N. Gau, Y. Hahn, and J. A. Retter, J. Quant. Spectrosc. Radiat. Transfer **23**, 147 (1980).
[14]M. H. Chen, Phys. Rev. A **34**, 1073 (1986).
[15]I. P. Grant, B. J. McKenzie, P. H. Norrington, D. F. Mayers, and N. C. Pyper, Comput. Phys. Commun. **21**, 207 (1980).
[16]H. A. Bethe and E. E. Salpeter, *Quantum Mechanics of One- and Two-Electron Systems* (Springer, Berlin, 1957).
[17]J. B. Mann and W. R. Johnson, Phys. Rev. A **4**, 41 (1971).
[18]U. Fano, Phys. Rev. **140**, A67 (1965).
[19]I. P. Grant, J. Phys. B **7**, 1458 (1974).
[20]M. E. Riley and D. G. Truhlar, J. Chem. Phys. **63**, 2182 (1975).
[21]D. Schneider (private communication).